Uniform Laser-Driven Relativistic Electron Layer for Coherent Thomson Scattering

H.-C. Wu (武慧春),[1,*] J. Meyer-ter-Vehn,[2] J. Fernández,[1] and B. M. Hegelich[1,3]

[1]*Los Alamos National Laboratory, Los Alamos, New Mexico 87545, USA*

[2]*Max-Planck-Institut für Quantenoptik, D-85748 Garching, Germany*

[3]*Department für Physik, Ludwig-Maximilians-Universität München, D-85748 Garching, Germany*

(Received 15 March 2010; published 8 June 2010)

A novel scheme is proposed to generate uniform relativistic electron layers for coherent Thomson backscattering. A few-cycle laser pulse is used to produce the electron layer from an ultrathin solid foil. The key element of the new scheme is an additional foil that reflects the drive-laser pulse, but lets the electrons pass almost unperturbed. Making use of two-dimensional particle-in-cell simulations and well-known basic theory, it is shown that the electrons, after interacting with both the drive and reflected laser pulses, form a very uniform flyer freely cruising with a high relativistic γ factor exactly in the drive-laser direction (no transverse momentum). It backscatters the probe light with a full Doppler shift factor of $4\gamma^2$. The reflectivity and its decay due to layer expansion are discussed.

DOI: 10.1103/PhysRevLett.104.234801 PACS numbers: 41.75.Jv, 41.60.−m, 42.55.Vc, 52.59.Ye

High-quality x-ray sources are requested in many fields of science. Presently, large free-electron lasers [1] represent powerful coherent extreme-ultraviolet and x-ray sources, which open a new era of intense extreme-ultraviolet or x-ray interaction with matter and provide unprecedented opportunities for research in condensed matter physics, high-energy-density physics [2], and single biomolecular imaging [3]. High laser harmonics from gas targets [4] and relativistic laser plasma interaction [5] are also very useful and promising coherent x-ray sources. Such harmonic sources typically produce trains of sharp spikes separated by the time period of the driving laser pulse.

Bright and coherent x-ray sources can also be obtained by coherent Thomson scattering (CTS) from dense electron layers flying with a relativistic factor $\gamma_x = 1/\sqrt{1-\beta_x^2}$. Here $\beta_x = v_x/c$ is the velocity of the plane flyer in the normal direction. A counterpropagating probe light is then mirrored and frequency upshifted by the relativistic Doppler factor, which is $(1+\beta_x)/(1-\beta_x) \approx 4\gamma_x^2$ for $\gamma_x \gg 1$ [6]. In this Letter we refer to these electron layers as relativistic electron mirrors (REMs), or simply flyers. One way to produce them is to drive cold nonlinear plasma waves to the point of wave breaking. Their density profile then develops diverging spikes that may move with high γ_x factors [7]. Recent experiments have demonstrated $\gamma_x \approx 5$ by identifying the mirrored light [8]. This method is limited by the phase velocity of the plasma wave requiring a low plasma density for high γ_x factors of the wave. Higher densities can be achieved by accelerating thin solid foils. Corresponding simulations were reported recently [9], driving a 250 nm thick foil with a laser intensity of about 10^{23} W/cm^2. Only small γ_x values are obtained in this case, because the complete foil including ions is accelerated.

In this Letter, a different regime is considered requiring much lower laser intensities and foils thin enough for the laser pulse to push out all electrons from the foil. In this case, only electrons are accelerated and can gain high γ values, while the heavy ions are left behind unmoved. For this to happen, the normalized laser field $a_0 = eE_{L,0}/mc\omega_L$ has to be much larger than the normalized field arising from charge separation, $E_{x,0} = (n_e/n_c)k_L d$. Here $\omega_L = ck_L$ is the circular frequency of the driving laser pulse, n_e is the electron density, and d the thickness of the foil initially, while $n_c = \epsilon_0 m_e \omega_L^2/e^2$ is the critical density. This regime has been described by Kulagin *et al.* in a number of papers (see, e.g., [10]), and CTS from the emerging relativistic electron layers has been studied in [11,12]. Some typical results are shown in Fig. 1. The scheme requires extremely thin foils of a few nanometers and laser pulses with a very high contrast ratio in order not to destroy the target before the main pulse arrives. These foils are much thinner than the skin depth and are therefore transparent, even though the electron density is overcritical. The leading edge of the laser pulse ionizes the foil and takes the electrons along as a thin sheath [see Figs. 1(a) and 2]. Their motion is well described in a single-electron picture [13,14]; transverse and longitudinal momenta follow approximately the local laser vector potential $a(x,t)$ according to $p_\perp = a$, $p_x = \gamma - 1 = a^2/2$, where γ is now the full relativistic factor.

There are two severe drawbacks when using these flyers as REMs for reflecting the probe light. First, the flyer $\gamma(t)$ depends on time such that the reflected pulse is chirped and has a broad spectrum. Second, the mirror γ_x is much smaller than the full γ for $\gamma \gg 1$ [see Fig. 1(b)]. In fact, we find for the Doppler shift

$$4\gamma_x^2 = 4\gamma^2/(1+p_\perp^2) \approx 2\gamma. \quad (1)$$

Apparently, the transverse momentum $p_\perp$, inherent to electron motion in transverse light waves, degrades the upshift. This is true even though the angle of electron motion relative to the laser direction, $\tan\theta = p_\perp/p_x = 2/a$, tends to vanish for large a.

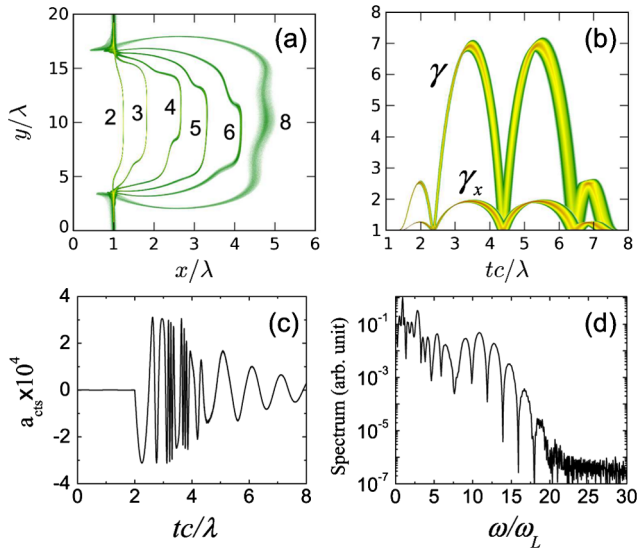

FIG. 1 (color online). Laser-driven electron layer blown out from a thin foil at $x/\lambda = 1$ by a drive-laser pulse incident from the left in the $(+x)$ direction and reflected light from a probe pulse incident from the right in the $(-x)$ direction. (a) Simulated electron density in the (x, y) plane given at different times in units of c/λ; (b) temporal evolution of γ_x and γ; (c) probe light reflected from the electron layer as seen by an observer at $x/\lambda = 6$; (d) corresponding spectrum.

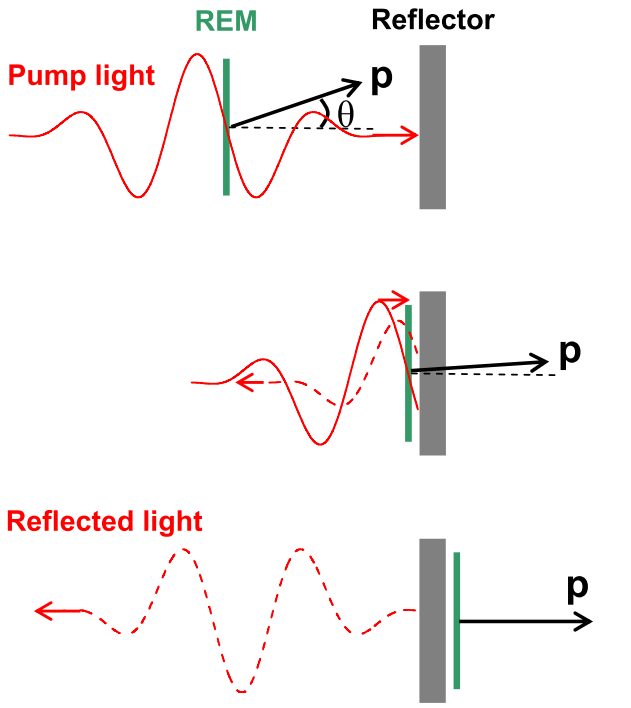

FIG. 2 (color online). Schematic drawing of electron layer (green) surfing on laser drive pulse and reflector foil (grey). The electron momentum is tilted by angle θ relative to the laser pulse axis. Middle part: The drive pulse is reflected by the reflector foil and interacts a second time with the electron layer. Lower part: The fully reflected drive pulse propagates to the left, while the electron layer has passed the reflector foil and is cruising to the right at a constant velocity and free of transverse momentum.

The major result reported in this Letter is a method to overcome these two drawbacks and to describe a practical way to generate flyers that have fixed γ values and $\gamma_x \approx \gamma$. Accordingly, they can produce optical pulses that are Doppler shifted by the full factor $4\gamma^2$ and have a narrow spectrum. They are only limited by decreasing reflectivity due to decay of the flyer. The way to suppress the transverse momentum is to let the electrons interact with a counterpropagating laser pulse. Here the central new observation is that the reflection of the drive pulse from a perfect mirror provides the ideal interaction pulse. The corresponding configuration is sketched in Fig. 2. Because of relativistic kinematics, the reflected pulse changes the energy γ of the flyer electrons only marginally, but eliminates their transverse momentum $p_\perp$ completely. While the electrons gain energy $(\Delta\gamma)^+ \propto a^2$ when comoving with the driving pulse for a long time, the interaction time with the reflected counterpropagating pulse is quite short, and, accordingly, the energy loss is only of order unity, $(\Delta\gamma)^- \propto 1$; this we have discussed in more detail in Ref. [11]. The change of transverse momentum can be expressed as $\Delta p_\perp = -e\int_{\tau_0}^{\tau_R} E_L(\tau)d\tau$; for a recent reference, see the book [13] and Chapters 1 and 5 therein. Here $E_L(\tau)$ represents the laser field, $\tau = t - x/c$ the propagation coordinate, and (τ_0, τ_R) the interaction interval. For the present case of reflection from a perfect mirror, it turns out that each electron passes the laser pulse 2 times, picking up identical changes in transverse momentum from both interactions, $(\Delta p_\perp)_{\text{refl}} = -\Delta p_\perp$, except for a minus sign due to the phase jump of π upon reflection. For both interactions, τ_0 denotes the front of the pulse and τ_R the coordinate the electron has when passing the reflector.

As a result, we find that the two momenta obtained from interaction with drive pulse and reflected pulse exactly cancel each other such that the electron emerging from behind the reflector foil has $p_\perp = 0$ and therefore $\gamma_x = \gamma$. Apparently, this result holds for each individual electron of the flyer independent of its initial distance from the reflector and the laser pulse shape $E_L(\tau)$. It is also independent of any longitudinal electric fields E_x, because these do not interfere in $\Delta p_\perp$. Such fields arise due to charge separation in the flyer and eventually cause longitudinal dispersion of the mirror. A different way to understand the cancellation of the transverse momentum is to recall that $p_\perp = \Delta p_\perp + (\Delta p_\perp)_{\text{refl}}$ can be expressed by the vector potential a of the laser wave and that, due to planar symmetry, the invariance $p_\perp = a$ still holds for the combined fields of forward-going and reflected pulse. Therefore $p_\perp \to 0$ since $a \to 0$ when passing the reflector.

We have checked these results by two-dimensional particle-in-cell simulations [15]. Figure 1 exhibits electron expulsion from a thin foil and CTS of a probe light from the emerging electron flyer for the case without a reflector. Here the simulation box has a size of $10\lambda \times 20\lambda$ in the xy plane, and a space resolution of 1000 cells/λ and

800 cells/λ in the x and y direction, respectively. The pump laser pulse has a profile $a_0 \sin^2(\pi t/T)$ with pulse duration $T = 3\lambda/c$. The carrier-envelope phase of the laser is set to zero so that the electric field maximum is at the pulse center. The transverse profile is chosen as a super-Gaussian $\exp(-r^4/R^4)$ with waist $R = 5\lambda$. We take $a_0 = 3.5$, corresponding to an intensity of $I = 2.6 \times 10^{19}$ W/cm^2 for $\lambda = 800$ nm. Few-cycle pulses of this strength are presently becoming available [16]. The laser pulse is linearly p polarized along the y direction and injected into the simulation box from the left boundary at $t = 0$. For this exploratory simulation, the initial ultrathin foil is chosen with density $n_e/n_c = 1$ and thickness $L/\lambda = 0.001$ and is located at $x_0 = 1\lambda$. Notice that even thinner layers of monoatomic carbon (graphene) are now available. The initial plasma temperature is 10 eV, and the ions are taken as immobile. The total number of macroparticles is about 5×10^7.

The electron density evolution is shown in Fig. 1(a). An electron layer is driven out of the foil (immobile ions at $x/\lambda = 1$ not shown), and one may notice some transverse electron motion in a polarization (y) direction superimposed on the drift in a laser (x) direction. Because of the transverse shaking, the effective area available for CTS is limited to the central zone within $9 < y/\lambda < 11$. The temporal evolution of γ and γ_x is shown in Fig. 1(b) for electrons located within $9.5 < y/\lambda < 10.5$. The energy spread of the electron layer increases with time and eventually leads to gradual longitudinal expansion. One also notices the conspicuous difference between γ and γ_x. The maximum values $\gamma_{\max} \approx 7.0$ and $\gamma_{x,\max} \approx 1.8$ agree with the single-electron prediction $\gamma_x \approx \sqrt{\gamma/2}$ [see Eq. (1)]. The evolution of $\gamma(t)$ follows approximately the laser vector potential according to the single-electron expression $\gamma(t) = 1 + a[x(t), t]^2/2$. After $t = 8\lambda/c$, the laser pulse has overtaken the electrons, which then return to rest in agreement with the Lawson-Woodward theorem [17].

Signatures of the probe light incident from the right side and backscattered from the relativistic electron layer are also shown in Fig. 1. In the simulation, the probe pulse is taken as a plane wave, $a_p(x, t) = a_{p0} \cos(k_L x + \omega_L t)$, and s polarized (in the z direction) to distinguish it from the drive pulse. A relatively small amplitude $a_{p0} = 0.1$ is chosen to make sure that the scattering is linear and that the flyer shape is not strongly perturbed. The reflected light is recorded by a fictitious observer located at $(x, y) = (6\lambda, 10\lambda)$. The temporal shape and spectrum of the reflected signal are shown in Figs. 1(c) and 1(d), respectively. By adjusting the time delay, we make sure that the fronts of both the pump and probe pulse touch the production foil at the same time. The reflected signal therefore contains the whole information on the flyer dynamics. Since the Doppler shift $4\gamma_x(t)^2$ varies with time, a complex oscillation pattern is observed in the reflected signal, leading to the broad spectrum seen in Fig. 1(d); the cutoff appears at $\omega/\omega_L = 4\gamma_x^2 \approx 16$ in agreement with the peak values of $\gamma_x \approx 2$. The two groups of rapid oscillations represent the two γ_x peaks in Fig. 1(b) and cause the spectral beating with period $\Delta\omega/\omega_0 \approx 2$. Though interesting as a diagnostics of flyer dynamics, such CTS pulses are of little value as a light source.

These results change drastically when adding the reflector foil. The configuration is illustrated in Fig. 2. Simulation results corresponding to those in Fig. 1, but now including the reflector, are depicted in Fig. 3. This figure highlights the central results of this Letter. It is observed that the electrons emerge from the reflector foil [marked by the dashed line in Fig. 3(a)] as a smooth dense layer in distinct contrast to the distorted shape seen in Fig. 1. In Fig. 3(b) one sees γ_x sharply rising and almost exactly merging with γ at a value of $\gamma_x = \gamma \approx 5.9$, while γ itself drops only by $\Delta\gamma \approx 1$. This is due to the interaction with the reflected drive pulse. As predicted above on the basis of single-electron motion, interaction with the reflected pulse fully eliminates transverse electron momentum, while reducing electron energy only marginally.

Although these sudden changes occur close to the reflector foil, it is important to understand that they are not due to any direct action of the reflector foil on the electrons, but are mediated indirectly by the reflected laser field. The reflector foil is modeled here as a fully ionized plasma slab with a density of $n_{e,R}/n_c = 400$ and a thick-

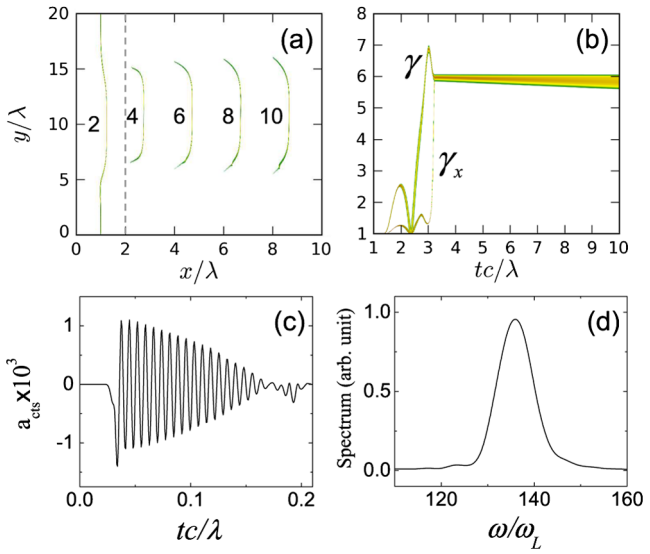

FIG. 3 (color online). Same as Fig. 1, but now including the 24 nm thick reflector foil. (a) A very uniform electron layer is emerging from the reflector foil (dashed line at $x_R/\lambda = 2$). (b) At about $t \approx 3c/\lambda$, when the electron flyer passes the reflector foil, γ_x approaches γ, indicating elimination of transverse electron momentum; the electron energy is given by nearly constant $\gamma = \gamma_x \approx 5.9$, and the energy spread increases slightly with time indicating layer expansion. (c) The reflected probe light appears as a regular, Doppler-compressed light wave that decays due to decreasing reflectivity of the expanding electron layer. (d) The spectrum shows a narrow x-ray pulse Doppler shifted by $4\gamma_x^2 \approx 139$ corresponding to a wavelength of 5.7 nm for a 800 nm probe light. For more details see text.

ness of $L_R/\lambda = 0.03$. This is sufficient to fully reflect the drive pulse. A reflectivity of 99.8% is obtained in the simulation. On the other hand, the relativistic electron layer passes the thin reflector foil practically unperturbed. The relative energy loss due to Coulomb collisions is found to be negligible in the order of 10^{-5}.

It appears that a uniform relativistic electron flyer with constant γ is produced that can now act as a CTS mirror. Backscattering of the probe light by this mirror has been simulated, using the same parameters as for the results of Fig. 1, but now increasing space resolution in the x direction to 1500 cells/λ in order to resolve the CTS signal of much higher frequency and also enlarging the box length in the x direction to 15λ. The reflected signal now consists of a regular wave train strongly compressed by the moving mirror [see Fig. 3(c)] and with a spectral peak [see Fig. 3(d)], Doppler shifted by the factor $4\gamma_x^2 = 4\gamma^2 \approx 139$ in best agreement with $\gamma = 5.9$. Here the observation point has been moved to $(x, y) = (13\lambda, 10\lambda)$ to record the full CTS signal. Although the probe light is incident continuously, the CTS signal decays due to the expansion of the flyer, which is clearly seen in Fig. 3(c). For an incident wavelength of $\lambda = 800$ nm, the x-ray pulse has a duration of about 500 attoseconds and a central wavelength of 5.7 nm. The maximum amplitude of $a_{\mathrm{cts}} = 1.4 \times 10^{-3}$ corresponds to an intensity of 4.2×10^{12} W/cm^2 and to a reflectivity of about 10^{-6}. By slightly changing the parameters, we expect that pulses of 10^9 coherent x-ray photons are possible, covering the spectral range of the water window.

The coherent reflectivity of these electron flyers has been studied in Ref. [12]. For a flyer density distribution $n_e(x) = n_0 S(x/d)$, given by a symmetric shape function $S(x/d) = S(-x/d)$ with characteristic thickness d and defined such that $n_e(0) = n_0$ and $\int n_e(x)dx = n_0 d$, the CTS amplitude in normal direction can be obtained as

$$a_{\mathrm{cts}} = a_{p0} \frac{\gamma(1+\beta)}{2} \frac{n_0 k_L d}{n_c} F(\xi) \qquad (2)$$

with the form factor $F(\xi) = \int_{-\infty}^{\infty} S(\chi)\cos(\xi\chi)d\chi$. Here $\chi \equiv x'/d'$ and $\xi \equiv 2k_L' d'$ denote normalized x coordinate and layer thickness in the rest frame of the electron flyer; in the lab frame ξ is given by $\xi = 2\gamma^2(1+\beta)k_L d$. A similar form factor $F(\xi)$ appears in the theory of coherent synchrotron radiation [18]. For a Gaussian profile $S(\chi) = \exp(-\pi\chi^2)$, we find $F(\xi) = \exp[-\xi^2/(4\pi)]$. Apparently, for such a shape the reflected signal vanishes exponentially as soon as $\xi \gg 1$; i.e., when the flyer becomes thicker than the wavelength of the reflected pulse. This implies that $d \gg \lambda/4\gamma^2$. For the parameters studied above, we have $n_0 = 0.252 n_c$, $d = 0.003\lambda$ (Gaussian fitting), and $\gamma = 5.96$, and obtain $a_{\mathrm{cts}} = 1.6 \times 10^{-3}$ in reasonable agreement with the particle-in-cell result shown in Fig. 3(c). The conversion ratio of pulse energy is found from Eq. (3) as

$$\alpha = \frac{(1+\beta)^2}{4}\left(\frac{n_0 k_L d}{n_c}\right)^2 F(\xi)^2. \qquad (3)$$

In conclusion, we have described a new method to make high-quality, microscale, relativistic electron mirrors. Dense electron layers, driven out from nanometer-thick production foils by few-cycle laser pulses, are significantly improved by introducing an additional reflector foil that reflects the drive-laser pulse, but lets the electrons pass unperturbed. As a result, very uniform relativistic electron layers are obtained, freely cruising at fixed high-γ values precisely in the drive-laser direction and with zero transverse momentum. Here we have discussed coherent Thomson backscattering from these layers to generate monochromatic, coherent, soft x-ray pulses, Doppler-shifted by a factor $4\gamma^2$. The goal was to explain basic features in terms of single-electron dynamics and verifying the scheme by two-dimensional particle-in-cell simulation. The next step will be experimental demonstration. Though demanding, both the generation of the required high-contrast laser pulses and the fabrication of the microscale double foil targets should be within range in the future. Successful demonstration would provide a new versatile tool for generating powerful laserlike x-ray pulses on a microscale.

The authors are grateful to Dr. Lin Yin for useful discussions. We also acknowledge a very helpful discussion with Dr. Chengkun Huang concerning the cancellation of transverse momentum. J. Meyer-ter-Vehn and H.-C. Wu were supported by the Munich Center for Advanced Photonics (MAP) and by the Association EURATOM–Max-Planck-Institute for Plasma Physics.

*hcwu@lanl.gov

[1] W. Ackermann *et al.*, Nat. Photon. **1**, 336 (2007).
[2] R. W. Lee *et al.*, J. Opt. Soc. Am. B **20**, 770 (2003).
[3] R. Neutze *et al.*, Nature (London) **406**, 752 (2000).
[4] J. Seres *et al.*, Nature (London) **433**, 596 (2005).
[5] B. Dromey *et al.*, Phys. Rev. Lett. **99**, 085001 (2007).
[6] A. Einstein, Ann. Phys. (Leipzig) **322**, 891 (1905).
[7] S. V. Bulanov, T. Zh. Esirkepov, and T. Tajima, Phys. Rev. Lett. **91**, 085001 (2003).
[8] A. S. Pirozhkov *et al.*, Phys. Plasmas **14**, 123 106 (2007).
[9] T. Zh. Esirkepov *et al.*, Eur. Phys. J. D **55**, 457 (2009).
[10] V. V. Kulagin *et al.*, Phys. Rev. Lett. **99**, 124801 (2007).
[11] J. Meyer-ter-Vehn and H.-C. Wu, Eur. Phys. J. D **55**, 433 (2009).
[12] H.-C. Wu and J. Meyer-ter-Vehn, Eur. Phys. J. D **55**, 443 (2009).
[13] H. K. Avetissian, *Relativistic Nonlinear Electrodynamics* (Springer, New York, 2006).
[14] M. Wen, J. Meyer-ter-Vehn, H.-C. Wu, and B. Shen, Eur. Phys. J. D **55**, 451 (2009).
[15] H.-C. Wu, Z.-M. Sheng, and J. Zhang, Phys. Rev. E **77**, 046405 (2008); New J. Phys. **10**, 043 001 (2008).
[16] K. Schmid *et al.*, Phys. Rev. Lett. **102**, 124801 (2009).
[17] P. M. Woodward, J. Inst. Electr. Eng. **93**, 1554 (1947); J. D. Lawson, IEEE Trans. Nucl. Sci. **26**, 4217 (1979).
[18] G. P. Williams *et al.*, Phys. Rev. Lett. **62**, 261 (1989).